NUMERICAL INVESTIGATION ON THE INFLUENCE OF TURBULENCE FLUCTUATIONS OVER WIND ENGINEERING PROBLEMS USING LARGE EDDY SIMULATION AND A SYNTHETIC INFLOW TURBULENCE GENERATOR

Alexandre Luis Braun, Deborah Madalozzo, Armando Miguel Awruch

PPGEC/UFRGS, Graduate Program in Civil Engineering, Federal University of Rio Grande do Sul, Av. Osvaldo Aranha 99, 90035-190, Porto Alegre – RS, Brazil, http://www.ufrgs.br/engcivil/ppgec/

Keywords: Large Eddy Simulation (LES), Synthetic turbulence, Computational Wind Engineering (CWE), Finite Element Method (FEM).

Abstract. A numerical investigation to study the influence of inflow turbulence fluctuations over predictions obtained from wind engineering applications using Large Eddy Simulation (LES) is performed in this work. It is well known that accurate LES results can be obtained if the inflow boundary conditions imposed on the computational domain satisfy prescribed spatial correlations and other turbulence characteristics. In order to reproduce experimental predictions obtained from wind tunnel tests and full-scale measurements, a synthetic turbulence generator is adopted here to produce velocity fluctuations over a specified region of the inflow plane considering the von Karman spectrum and the divergence-free condition. A numerical model based on the Finite Element Method (FEM) and the explicit two-step Taylor-Galerkin algorithm is employed in this work to simulate wind flows, where turbulence is also simulated by using LES with the classic and dynamic sub-grid scale models. Some numerical analyses are carried out with the present scheme and results are compared with experimental and numerical predictions obtained by other authors.

1   INTRODUCTION

Evaluation of wind loads and its effects is crucial for designing long-span bridges, tall buildings and other structures subject to damages induced by the wind action. Recent investigations have been conducted using numerical models based on conventional Computational Fluid Dynamics (CFD) and fluid-structure interaction algorithms (see, for instance, Braun and Awruch, 2005; Braun and Awruch, 2009a), where the fluid and structure motions are evaluated simultaneously by considering some coupling formulation (see Braun and Awruch, 2009b). Owing to constant improvements observed in the computational resources utilized by numerical simulations, such as processing power and storage capacity, Large Eddy Simulation (LES) has been widely applied to Computational Wind Engineering (CWE), where wind engineering problems are investigated numerically (see, for instance, Tamura, 2008). An important issue related to turbulence flows observed in CWE is related to generating velocity fluctuations to reproduce turbulence statistics over the simulated flow.

Inflow boundary conditions are very important to obtain accurate results when numerical simulations of wind engineering problems are carried out. In earlier studies, smooth uniform flows were usually considered in order to avoid numerical difficulties related to inflow and outflow prescriptions. Nevertheless, for direct comparison with experimental and field predictions, simulations of natural wind flows must be performed considering turbulence fluctuations in the incident stream, which are usually induced by obstacles located upstream the investigated body.

For Reynolds Averaged Navier-Stokes (RANS) approaches only mean profiles describing the flow velocity and turbulence parameters are specified, leading to straightforward definition of inlet flow conditions. On the other hand, the application of LES in computational wind engineering requires special techniques to impose unsteady inflow boundary conditions, where some method to generate realistic velocity fluctuations must be utilized.

According to Keating et al. (2004), all methods to generate velocity fluctuations can be classified into three major groups: recycling methods, precursor databases and synthetic turbulence. Basically, the simplest way to generate these velocity fluctuations is to store data from a previous LES computation (see Mochida et al., 1993). Another alternative is to obtain artificial velocity fluctuations given by the inverse Fourier transform of a prescribed energy spectrum with target turbulence intensity and length scale, where series of trigonometric functions are adopted considering wave superposition. The simulation schemes can be also characterized as Gaussian or non-Gaussian, homogeneous or non-homogeneous and one-dimensional or multi-dimensional processes.

Precursor approaches lead to more realistic flows, considering that accurate inlet boundary conditions for turbulent flows can be easily obtained using a precursor simulation in order to store time series of velocity fluctuations. Rectangular prisms, with dimensions adjusted according to the desired conditions, positioned upstream of the immersed body are also utilized to generate velocity fluctuations (see Tamura et al., 2002). However, the precursor technique is restricted to simple cases and therefore the method is not adequate for general applications. In addition, it requires extra computational load and significant storage resources. On the other hand, digital filtering offers efficient methods for simulating random processes, where integration of a differential equation driven by white noise is performed. In the work of Bilson et al. (2004), an algorithm to prescribe turbulent time and length scales independently is presented and an asymmetric time filter is suggested. Another method to filter random data was proposed by Klein et al. (2003). In this sense, many authors have used Gaussian filters to generate inflow data with spatial as well as temporal correlations, such that non-homogeneous turbulence can be reproduced. Unfortunately, turbulence statistics such as

spatial correlations and turbulence intensities related to preliminary computations may not correspond to prescribed target characteristics. For further details on recycling and precursor approaches, readers are addressed to Liu and Pletcher (2006).

Recent studies have focused on methods for generating fluctuations using synthetic turbulence. The main objective of synthetic turbulence generators is to eliminate the need for a transition domain required by precursor schemes in order to make the flow realistic. The first models were developed by authors such as Shinozuka (1971), Shinozuka and Jan (1972) and Hoshiya (1972), who employed an inverse Fourier transform based on prescribed power spectral density and cross-spectral density to obtain time series of wind velocity fluctuations, which were described by trigonometric series with random coefficients. It is relevant to notice that the use of Fourier series to express wind speed fluctuations was formerly suggested by Davenport (1961).

Initial studies focused on the generation of one-dimensional processes. One of the first techniques to simulate processes with more than a single dimension was presented by Shinozuka (1971), where a target energy spectrum is approximated in a discrete sense by superposition of trigonometric functions with random phase angles. An essential assumption of Shinozuka's method is that a random process can be simulated by a series of cosine functions with random frequency or wave number. The density function of the random frequency is derived from the specified cross-spectral density matrix for multivariate process or from the specified spectral density function for multidimensional process. Unfortunately, the scheme becomes computationally inefficient for a large number of variables. Nevertheless, a realistic model for natural wind requires the superposition of three orthogonal and cross-correlated fields of the wind velocity.

Shinozuka and Jan (1972) presented a method to simulate a multivariate multidimensional stochastic process, where the modeling of atmospheric turbulence was highlighted. The proposed method is able to calculate a discrete inverse Fourier transform efficiently, although reference to phase has not been made. A given spectral density function or the target spectrum is adopted to weight a sum of cosine terms and frequencies can be jittered to reduce the degree of periodicity in the time series. Since the method employs a discretized target spectrum, some frequencies are absent while others are over emphasized. One can observe that the greater the range of frequencies covered in the target spectrum, the greater the number of terms needed in the series.

Kondo et al. (1997) adopted the wave superposition approach in conjunction with a fast Fourier transform (FFT) to simulate velocity fluctuations for LES. Amplitudes of the Fourier modes were computed from the target spectrum and phases are obtained randomly. Missing phase information related to real turbulent eddies leads to less accurate results. Moreover, an additional step was required to enforce the divergence-free condition, which deviated the resulted power spectral density from the target spectrum.

Isotropic synthesized fluctuations based on the method introduced by Kraichnan (1970) have been adopted to generate turbulent fluctuations. Further developments have been proposed by several researches such as Li et al. (1994), Smirnov et al. (2001), Klein et al. (2003), Batten et al. (2004) and Davidson (2007). In this method, an energy spectrum is prescribed to obtain the amplitude of fluctuations as a function of the wave number. Non-isotropic fluctuations have been investigated by authors such as Le and Moin (1994) and Batten et al. (2004), where some techniques are employed to scale the synthesized fluctuations generated previously in order to reproduce a prescribed Reynolds stress tensor. However, the scaling procedure modifies the prescribed spectrum if the Reynolds stress tensor is non-homogeneous, which is always observed for real flows.

More recently, Jarrin et al. (2006) proposed a method to generate turbulence based on prescribing a superposition of coherent structures instead of using spectral techniques, where eddies are generated randomly considering a shape function localized in space, which are convected through the inlet plane. Huang et al. (2010) presented a general inflow turbulence generator able of generating spatially correlated turbulent flow fields, which satisfy the von Karman model or an arbitrary spectrum. The proposed scheme is based on the discretizing and synthesizing random flow generation (DSRFG) technique, which satisfies the divergence-free condition without supplementary steps. In addition, the method can reproduce non-homogeneous and anisotropic turbulent flows.

In the present work, a numerical model based on the explicit two-step Taylor-Galerkin method is utilized to simulate incompressible flows. The pseudo-compressibility hypothesis is applied over the mass conservation equation in order to obtain the pressure field explicitly. Turbulence is analyzed considering LES with the classic and dynamic sub-grid scale models, where velocity fluctuations are produced with a synthesized turbulence generator, which is able to reproduce isotropic homogeneous turbulence with a velocity field spatially and temporally correlated. The finite element method (FEM) is adopted for spatial discretizations, where eight-node hexahedral elements with one-point quadrature are employed. A simple and idealized example is initially considered for evaluation of turbulence statistics concerning the fluctuating field generated by the proposed method over the flow domain. Lastly, a full-scale building is simulated in order to apply the numerical model to a typical Computational Wind Engineering application.

2   THE FLOW GOVERNING EQUATIONS

The governing equations for a general fluid flow are obtained from momentum, mass and energy balances over the spatial domain where the problem takes place, which may be simplified when some physical assumptions concerning the fluid/flow behavior are made. In the field of CWE, wind flows are usually described with the following assumptions:

1) Natural wind streams are considered to be within the incompressible flow range;
2) Natural wind streams are considered to be within the turbulent flow range;
3) Wind is always flowing with a constant temperature (isothermal process);
4) Gravity forces are neglected in the fluid equilibrium;
5) Air is mechanically considered as a Newtonian fluid.

The governing equations of the fluid domain are then reduced to the well-known Navier-Stokes equations and the continuity equation (see White, 2005). An ALE (arbitrary Lagrangian-Eulerian) description is usually introduced in the fluid formulation in order to take into account interactions between fluid and structural motions when fluid-structure interaction problems are investigated (see, for instance, Braun and Awruch, 2009b). However, in the present work only aerodynamic simulations are carried out using a classical Eulerian kinematical description of the fluid motion. Numerical difficulties inherent to the simulation of incompressible flows are circumvented employing the pseudo-compressibility approach introduced by Chorin (1967), which leads to explicit evaluation of the pressure field. Consequently, the system of governing equations adopted here may be written as follows:

$$\frac{\partial v_i}{\partial t} + v_j \frac{\partial v_i}{\partial x_j} = \frac{1}{\rho} \frac{\partial \sigma_{ij}}{\partial x_j} \qquad (i, j = 1, 2, 3) \tag{1}$$

$$\frac{\partial p}{\partial t} + v_j \frac{\partial p}{\partial x_j} + \rho c^2 \frac{\partial v_j}{\partial x_j} = 0 \qquad (j = 1, 2, 3) \tag{2}$$

where v_i denotes components of the velocity vector according to the direction of the Cartesian axes x_i, p represents the thermodynamic pressure, ρ is the fluid density and c is the sound speed in the flow field. The system of governing equations introduced above is valid for a spatial domain Ω_f and a time interval T, where $t \in [0,T]$.

The components of the Cauchy stress tensor σ_{ij} may be decomposed into pressure and viscous parts as follows:

$$\sigma_{ij} = -p\delta_{ij} + \tau_{ij} \qquad (i, j = 1, 2, 3) \tag{3}$$

where δ_{ij} are components of the Kroenecker's delta ($\delta_{ij} = 1$ for $i = j$; $\delta_{ij} = 1$ for $i \neq j$) and τ_{ij} are components of the viscous stress tensor, which is expressed according to the Newtonian constitutive formulation and the Stokes hypothesis (see White, 2005), that is:

$$\tau_{ij} = \mu \left(\frac{\partial v_i}{\partial x_j} + \frac{\partial v_j}{\partial x_i} \right) + \lambda \frac{\partial v_k}{\partial x_k} \delta_{ij} \qquad (i, j, k = 1, 2, 3) \tag{4}$$

where μ and λ are the kinematical and volumetric viscosities of the fluid, respectively.

Neumann and Dirichlet boundary conditions must be specified on the boundary Γ_{Tf} to solve the flow problem, which are given by the following expressions:

$$v_i = \bar{v}_i \qquad (i = 1, 2, 3) \quad \text{on } \Gamma_f \tag{5}$$

$$p = \bar{p} \qquad \text{on } \Gamma_p \tag{6}$$

$$\left[-\frac{p}{\rho}\delta_{ij} + \frac{\mu}{\rho} \left(\frac{\partial v_i}{\partial x_j} + \frac{\partial v_j}{\partial x_i} \right) + \frac{\lambda}{\rho} \frac{\partial v_k}{\partial x_k} \right] n_j = \frac{\sigma_{ij}^f n_j}{\rho} = \bar{S}_i \quad (i, j, k = 1, 2, 3) \text{ on } \Gamma_\sigma \tag{7}$$

where Γ_f (boundary with prescribed values $\bar{v}_i$ for the fluid velocity field), Γ_p (boundary with prescribed values $\bar{p}$ for the pressure field), and Γ_σ (boundary with prescribed values $\bar{S}_i$ for the traction vector) are complementary subsets of boundary Γ_{Tf}, such that $\Gamma_{Tf} = \Gamma_f \cup \Gamma_p \cup \Gamma_\sigma$. In Eq. (7) n_j are components of the unit normal vector **n** at a point located on boundary Γ_σ. Initial conditions for the pressure and velocity fields must be also specified at $t = 0$ to start up the flow analysis.

3 TURBULENCE MODELING

Turbulent flows are very difficult to be numerically reproduced by CFD models because the smaller turbulence scales, which are associated with the smaller eddies of the flow field, require computational meshes with very fine resolution in order to describe correctly the motion associated with these flow structures. The turbulence problem is usually solved employing modified governing equations that reproduce statistically the turbulence effects over the main flow. These turbulence effects are represented by a turbulence model.

Turbulence modeling is performed in this work employing LES with the dynamic sub-grid scale model (Germano et al., 1991; Lilly, 1992). According to the classical LES methodology, the governing equations are submitted first to a spatial filtering process (Smagorinsky, 1963) where the flow field is decomposed into large and small scales (or large and small eddies). Large eddies are solved directly with the filtered equations, which are described by field variables associated with the large scales, and eddies smaller than the grid resolution are

modeled by turbulence closure models in order to represent the small scales effects over the large scales. After the filtering process, the Reynolds sub-grid stress tensor τ_{ij}^{SGS} is obtained, with its components given according to the Boussinesq assumption, that is:

$$\tau_{ij}^{SGS} = \rho\left(\overline{v_i' v_j'}\right) = 2\mu_t \overline{S}_{ij} \tag{8}$$

where apostrophes indicate sub-grid scale variables, μ_t is the eddy viscosity and $\overline{S}_{ij}$ are components of the strain rate tensor, which are expressed in terms of large scale variables. The components of the Reynolds sub-grid stress tensor must be added to the respective components of the viscous stress tensor to determine the final form of the momentum equations. The eddy viscosity μ_t is obtained here employing the dynamic sub-grid scale model, which may be expressed by:

$$\mu_t = \rho C(\vec{x}, t) \overline{\Delta}^2 \left|\overline{S}\right| \tag{9}$$

where $C(\vec{x}, t)$ is the dynamic coefficient (with $\vec{x}$ and t indicating space and time dependencies), $\left|\overline{S}\right|$ is the filtered strain rate tensor modulus and $\overline{\Delta}$ is the characteristic dimension of the grid filter, which is associated to the element volume in FEM formulations ($\overline{\Delta} = \sqrt[3]{element\ volume}$). The dynamic coefficient is updated along the time integration process taking into account instantaneous conditions of the flow field. If the dynamic coefficient is assumed to be constant, the Smagornsky's model is obtained. The solution of Eq. (9) demands two filtering processes on the flow governing equations: the first filtering is associated to the use of the LES formulation, which is related to the grid filter $\overline{\Delta}$ and the large scale variables represented by overbars ($\overline{\bullet}$). The second filtering process is referred to another filter called test filter $\langle\overline{\Delta}\rangle$, which must be larger than the first grid filter $\overline{\Delta}$. Variables are identified by the symbol $\langle\bullet\rangle$ after the second filtering process and they are computed here using the following expression (see Fig. 1):

$$\langle\overline{k}\rangle^i = \frac{\displaystyle\sum_{j=1}^{n}\left(\frac{\overline{k}^j}{d_i^j}\right)}{\displaystyle\sum_{j=1}^{n}\left(\frac{1}{d_i^j}\right)} \tag{10}$$

where $\langle\overline{k}\rangle^i$ is the value related to a generic variable $\overline{k}$ obtained by the second filtering process at the nodal point i, which is associated with large scales defined by the first filtering process, n is the number of nodal points having direct connectivity with the nodal point i, d_i^j is the distance between the nodal points i and j and $\overline{k}^j$ is the value related to a generic variable k computed with the first filtering process at the nodal point j. The characteristic dimension of the second filter, which is employed in the computation of the dynamic coefficient $C(\vec{x}, t)$, may be defined as $\langle\overline{\Delta}\rangle = 2*\overline{\Delta}$ for regularly spaced grids.
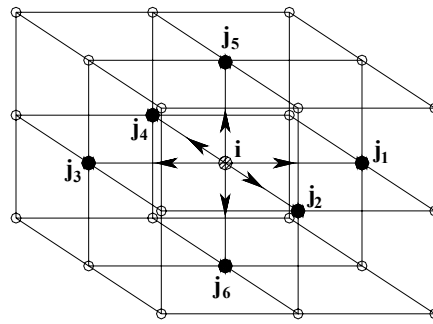
Figure 1. Second filter arrangement.

When turbulence fluctuations are considered in the incidence flow, the inflow boundary conditions are modified to include velocity fluctuations on the mean velocity field. In the present work, a synthetic turbulence generator proposed by Davidson (2007) is adopted, where fluctuations are obtained using N random Fourier modes as follows:

$$v_i'(x_j) = 2\sum_{n=1}^{N} \hat{v}^n \cos(\kappa_j^n x_j + \psi^n)\, \sigma_i^n \qquad (11)$$

where v_i' are components of the fluctuating velocity vector given according to the Cartesian directions x_i, which are defined at a specific point with coordinates x_j, and $\hat{v}^n$ and ψ^n are the amplitude and phase associated with the Fourier mode n, respectively. The wave number vector κ_j^n and the velocity unit vector σ_i^n, which also indicate the direction of the Fourier mode n, are orthogonal in the spatial domain for each wave number n, since the unit vector σ_i^n must satisfy continuity, that is $\sigma_i^n \kappa_i^n = 0$. The direction of σ_i^n in the plane $\xi_1^n - \xi_2^n$ is randomly obtained considering an angle α^n. Furthermore, σ_3^n must be parallel to ξ_3^n, indicating that σ_3^n is chosen to be parallel to κ_i^n (see Fig. 2). Angles φ^n and θ^n and phase φ^n are also obtained randomly.
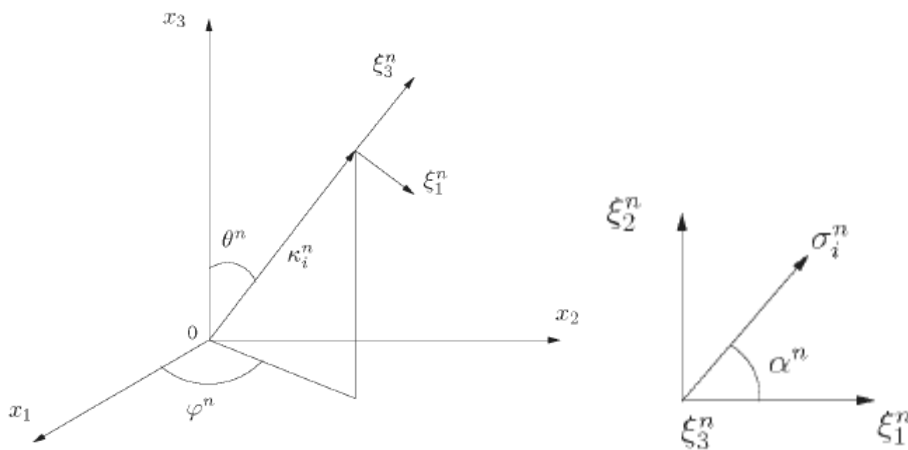
Figure 2 – Defining the wave number direction (Davidson, 2007).

Amplitude $\hat{v}^n$ is obtained for each mode by considering a modified von Karman spectrum as follows:

$$\hat{v}^n = \sqrt{E\left(\left|\kappa_j^n\right|\right)\Delta\kappa} \tag{12}$$

where:

$$E(\kappa) = 1.453\frac{v_{rms}^2}{\kappa_e}\frac{(\kappa/\kappa_e)^4}{\left[1+(\kappa/\kappa_e)^2\right]^{17/6}}e^{\left[-2(\kappa/\kappa_\eta)^2\right]} \tag{13}$$

with:

$$\kappa = \left(\kappa_i\kappa_i\right)^{1/2} \tag{14}$$

$$\kappa_\eta = \varepsilon^{1/4}v^{-3/4} \tag{15}$$

$$\kappa_e = 1.453\frac{9\pi}{55L_t} \tag{16}$$

where v_{rms} represents the standard deviation of the streamwise velocity, ε is the rate of energy dissipation, v is the kinematic viscosity and L_t is the turbulence length scale. Figure 3 shows the modified von Karman spectrum, where $\kappa_1 = \kappa_e/p$ is defined as the smallest wave number and $\Delta\kappa = (\kappa_{max} - \kappa_1)/N$ is the equally spaced wave number interval. The factor p is chosen to be larger than one in order to make the largest scales larger than those corresponding to κ_e. The highest wave number is defined considering the mesh resolution, that is $\kappa_{max} = 2\pi/(2\Delta)$, where Δ is the grid spacing.
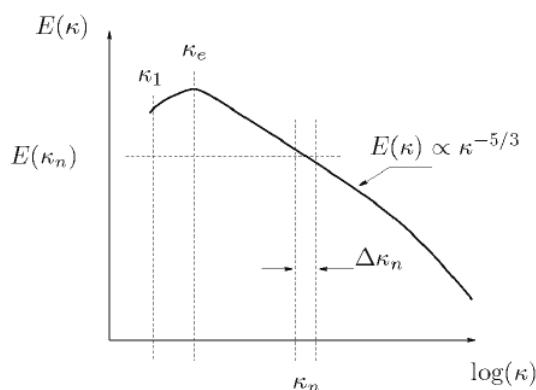
Figure 3 – The modified von Karman spectrum (Davidson, 2007)

In order to obtain a fluctuating velocity field with time correlation, since the fluctuations generated with the formulation presented above are independent of each other, a time filter must be employed over the response computed with Eq. (11). An asymmetric time filter may be adopted as follows (see Klein et al., 2003):

$$(\overline{v}_i')^n = a(\overline{v}_i')^{n-1} + b(v_i')^n \tag{17}$$

with:

$$a = e^{-\Delta t/\tau}; \qquad b = (1-a^2)^{1/2} \tag{18}$$

where n and n-1 denote the current and previous time steps, respectively, and τ is the turbulence time scale, which is usually approximated as:

$$\tau = \frac{L_t}{v_{rms}} \tag{19}$$

Further details on the numerical model adopted here to generate turbulence fluctuations are found in Davidson (2007).

The inlet boundary conditions corresponding to Eq. (5) are then rewritten as follows:

$$v_i = V_i + \overline{v}_i' \quad \text{on } \Gamma_v^{inlet} \tag{20}$$

where V_i are components of the time average velocity vector according to the Cartesian directions x_i and Γ_v^{inlet} denotes a specific area on the inlet plane where fluctuations take place, which is defined in order to avoid ill posed boundary conditions on the side and top planes of the computational domain.

One can observe that the inlet region of computational grids is usually covered by a reduced number of elements, such that the grid spacing may be larger than the turbulent length scale. Nevertheless, the main objective of all methods to introduce turbulence fluctuations in the flow field is to provide inflow boundary conditions instantaneously with correct turbulence properties, such as time and length scales, which will be only maintained if the grid presents adequate refinement. In other words, the inlet turbulence should have integral length and time scales related to the grid size and the time step adopted in the numerical analysis. Due to lack of large-scale energy-containing structures, the generated turbulence may be quickly dissipated.

Figure 4 shows the reproduction of the actual spectrum obtained from a realistic wind flow, which is compared with the respective spectra given by the Gaussian and von Karman models. It is observed that the spectral density corresponding to the generated turbulent flow follows approximately the Gaussian spectral model during the energy-containing sub-range. Since the energy-containing sub-range of turbulence contains the bulk of the turbulence energy and energy production in wind flows, the Gaussian model may be adopted as a first approximation.
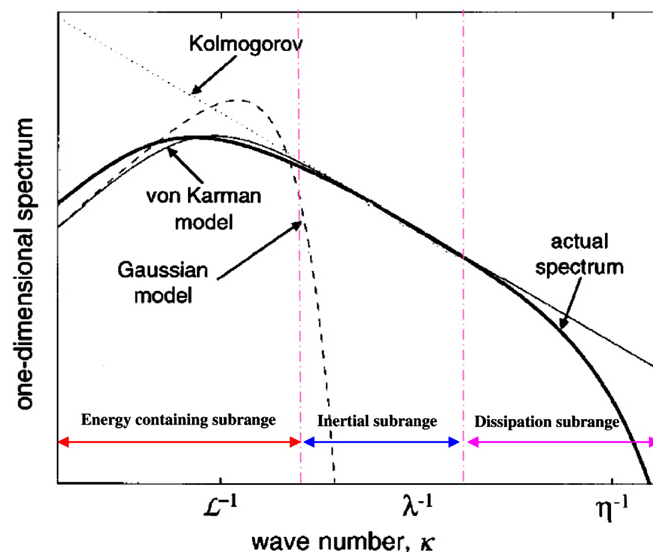
Figure 4 – Comparison between the von Karman spectrum and the Gaussian spectrum (Huang et al., 2010).

The energy contained in the dissipation range may be less significant for LES approaches, since the Kolmogorov scale is much smaller than the filtering length scale adopted by LES.

Nevertheless, the energy contained in the inertial sub-range, where energy is transferred from the large scales to the dissipation scale, may be important for LES because the corresponding length scale lies between the integral and the Kolmogorov scales. Since the filtering length scale utilized in LES is able to resolve a considerable amount of energy associated with the inertial sub-range, it cannot be neglected. Therefore, generation of fluctuating velocity fields must be performed satisfying the spectrum proposed by the von Karman model in order to obtain an accurate evaluation of wind effects when LES is carried out. According to experimental predictions (see Hinze, 1975; Simiu and Scanlan, 1996), the von Karman model is able to represent both the energy-containing and inertial subranges adequately for evaluations of the wind effects over buildings and other structures, where turbulent eddies associated with the inertial sub-range present a significant contribution to the wind-induced forces.

4   THE NUMERICAL MODEL

The solution field for the flow governing equations is obtained in this work employing a numerical model based on the explicit two-step Taylor-Galerkin scheme (Kawahara and Hirano, 1983; Braun, 2007). In this model, temporal derivatives are first approximated by Taylor series expansions up to second order terms and the Bubnov-Galerkin weighted residual method is then applied to the discretized equations in the context of the FEM (Zienkiewicz et al., 2005). Spatial dicretization is performed considering eight-node hexahedral elements with one-point point quadrature, where a stabilization scheme is adopted in order to avoid the incidence of spurious modes due to hourglass instability. For additional information on the numerical model adopted in this work see Braun (2007).

The algorithm for solution of the flow governing equations may be summarized as follows:

(I) Solve the momentum equations to obtain a first approximation for the velocity field at the intermediate point of the time step, that is $\bar{v}_i^{n+1/2}$:

$$\bar{v}_i^{n+1/2} = v_i^n + \frac{\Delta t}{2} \left\{ -v_j \frac{\partial v_i}{\partial x_j} - \frac{1}{\rho} \frac{\partial p}{\partial x_j} \delta_{ij} + \frac{\partial}{\partial x_j} \left[\frac{\mu + \mu_t}{\rho} \left(\frac{\partial v_i}{\partial x_j} + \frac{\partial v_j}{\partial x_i} \right) + \frac{\lambda}{\rho} \frac{\partial v_k}{\partial x_k} \delta_{ij} \right] + \left(\frac{\Delta t}{4} v_j v_k \right) \frac{\partial^2 v_i}{\partial x_j x_k} \right\}^n$$

where μ_t must be previously obtained from Eq. (9).

(II) Impose the boundary conditions specified by Eqs. (5) and (7) (or Eqs. 20 and 7) on the velocity field $\bar{v}_i^{n+1/2}$.

(III) Solve the mass conservation equation to obtain the pressure field at the intermediate point of the time step, that is $p^{n+1/2}$:

$$p^{n+1/2} = p^n + \frac{\Delta t}{2} \left\{ \left[-v_j \frac{\partial p}{\partial x_j} - \rho c^2 \frac{\partial v_j}{\partial x_j} \right] + \left(\frac{\Delta t}{4} v_i v_j \right) \frac{\partial^2 p}{\partial x_j \partial x_i} \right\}^n$$

(IV) Impose the boundary condition specified by Eq. (6) on the pressure field $p^{n+1/2}$.

(V) Determine the pressure increment:

$$\Delta p^{n+1/2} = p^{n+1/2} - p^n$$

(VI) Determine the corrected velocity field using the pressure increment obtained above, that

is $v_i^{n+1/2}$:

$$v_i^{n+1/2} = \overline{v}_i^{n+1/2} - \frac{1}{\rho} \frac{\Delta t^2}{8} \frac{\partial \Delta p^{n+1/2}}{\partial x_i}$$

(VII) Impose the boundary conditions specified by Eqs. (5) and (7) (or Eqs. 20 and 7) on the corrected velocity field $v_i^{n+1/2}$.

(VIII) Update the velocity field using $v_i^{n+1} = v_i^n + \Delta v_i^{n+1/2}$, where:

$$\Delta v_i^{n+1/2} = \Delta t \left\{ -r_j \frac{\partial v_i}{\partial x_j} - \frac{1}{\rho} \frac{\partial p}{\partial x_j} \delta_{ij} + \frac{\partial}{\partial x_j} \left[\frac{\mu + \mu_t}{\rho} \left(\frac{\partial v_i}{\partial x_j} + \frac{\partial v_j}{\partial x_i} \right) + \frac{\lambda}{\rho} \frac{\partial v_k}{\partial x_k} \delta_{ij} \right] \right\}^{n+1/2}$$

(IX) Impose the boundary conditions specified by Eqs. (5) e (7) (or Eqs. 20 and 7) on the updated velocity field v_i^{n+1} .

(X) Update the pressure field using $p^{n+1} = p^n + \Delta p^{n+1/2}$, where:

$$\Delta p^{n+1/2} = \Delta t \left\{ -r_j \frac{\partial p}{\partial x_j} - \rho c^2 \left(\frac{\partial v_j}{\partial x_j} \right) \right\}^{n+1/2}$$

(XI) Impose the boundary condition specified by Eq. (6) on the updated pressure field p^{n+1} .

(XII) Return to step I and proceed with the next time step until the time march ends.

Since the numerical model utilized in this work presents explicit nature, the time step adopted in the time discretization must be carefully determined in order to maintain numerical stability. The time step is limited to a specific value related to physical aspects associated with the sound propagation through the matter, which is obtained according to the well known Courant condition:

$$\Delta t = \alpha \frac{\Delta x_E}{V_E + c} \tag{21}$$

where Δx_E is the characteristic dimension of element E, V_E the characteristic velocity associated to element E, c is the sound speed in the physical medium and α is a safety coefficient, which is always smaller than unity. In the present work, the time step is defined taking into account the smaller time step obtained from Eq. (21), which is usually related to the smaller element of the finite element mesh.

5 NUMERICAL APPLICATIONS

5.1 Turbulence generation over a flat plate

A simple example is investigated here in order to verify the numerical model proposed in this work to generate turbulent flows based on inflow turbulence. Turbulence statistical data are determined considering the flow over a flat plate, where fluctuations are artificially produced by the synthesized turbulence generator model utilized in this paper. The main objective of the present study is to evaluate the influence of important aspects such as grid size as well as length and time scales on the numerical predictions referring to the turbulence

statistical parameters utilized to characterize the flow field. Eight tests are performed with different turbulence configurations, which descriptions are found in Table 1, where isotropic turbulence is assumed. The flow velocity components are measured at three different positions along the centerline of the computational domain: $x_1 = 0$ m; $x_1 = 15$ m; $x_1 = 30$ m. The spatial domain employed in the present investigation is geometrically characterized with 30 m length (x_1), 10 m width (x_2) and 10 m height (x_3), which is discretized considering two mesh refinements: Mesh 1, presenting 60x20x20 hexahedral elements with uniform grid spacing of 0.5 m ($\Delta x_1 = \Delta x_2 = \Delta x_3 = 0.5$ m), and Mesh 2, presenting 120x40x40 hexahedral elements with uniform grid spacing of 0.25 m ($\Delta x_1 = \Delta x_2 = \Delta x_3 = 0.25$ m). The boundary conditions can be summarized as follows: symmetry conditions are imposed on the side and top walls of the computational domain, no-slip boundary conditions are considered on the ground level and a constant pressure field ($p = 0$) is imposed on the outflow boundary. In addition, the inflow boundary condition is defined taking into account a uniform distribution for the longitudinal mean velocity component. Turbulence fluctuations are produced over a limited region referring to the inlet plane of the computational domain and superposed to the mean flow field since the first time step of the numerical analysis. It is important to notice that boundary layer effects are not evaluated in the present investigation, whereas the finite element mesh employed here is not supposed to reproduce turbulence instabilities associated with the plate surface. A schematic view of the problem analyzed here can be found in Figure 5, where the region for production of inflow turbulence is also defined. Flow and geometric constants utilized in the present analyses are given in Table 2.

		MESH1	MESH2
BDIST1		0.4 (T0); 1.5 (T1-T7)	0.4 (T0); 1.5 (T1-T7)
BDIST2		0.4 (T0); 1.5 (T1-T7)	0.4 (T0); 1.5 (T1-T7)
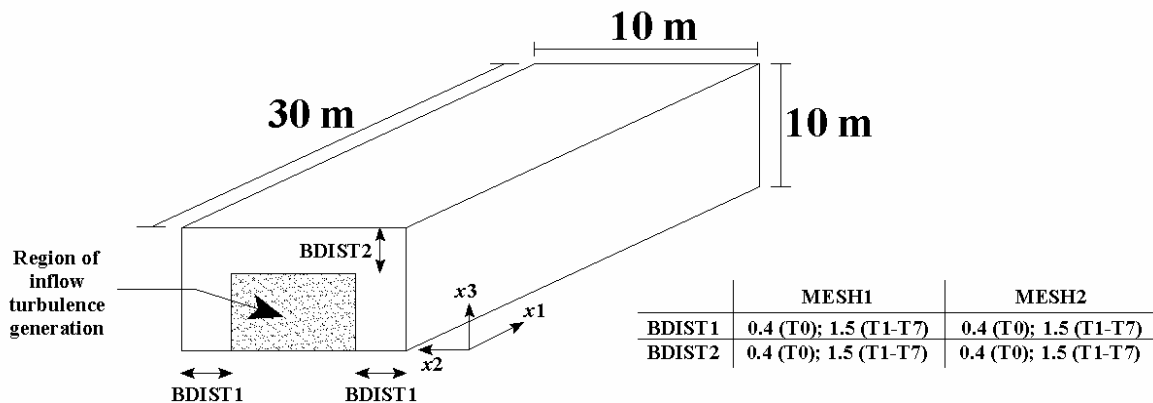
Figure 5. Geometric characteristics adopted in the flow analysis over a flat plate.

Tests	Turbulence length scale (L_t)	Turbulence intensity (I)	Factor p ($\kappa_1 = \kappa_e/p$)
T0	10 m	15%	4
T1	5 m	15%	4
T2	2.5 m	15%	4
T3	1 m	15%	4
T4	0.5 m	15%	4
T5	0.1 m	15%	4
T6	0.05 m	15%	4
T7	0.01 m	15%	4

Table 1. Turbulence parameters adopted in the flow analysis over a flat plate.

Constants	Mesh 1	Mesh 2
Fluid specific mass (ρ)	1.0 kg/m^3	1.0 kg/m^3
Kinematic viscosity (ν)	10^{-2} m^2/s	10^{-2} m^2/s
Sound speed (c)	100 m/s	100 m/s
Mean flow velocity	10 m/s	10 m/s
Time step (Δt)	2x10^{-3} s	1x10^{-3} s

Table 2. Flow and geometric constants utilized in the flow analysis over a flat plate.

Results referring to time histories of the flow velocity components are presented in Fig. 6 considering a measurement performed at the center point of the inflow plane ($x_1 = 0$ m; $x_2 = 5$ m; $x_3 = 5$ m) and the finite element discretization corresponding to Mesh 1. In addition, the corresponding energy spectra ($S(n)$) are also shown, where comparisons are carried out taking into account a target spectrum described according to the von Karman model (red line). One can observe that the influence of the prescribed length scales over the velocity fluctuations produced with the present scheme is clearly identified, since the amplitude of the velocity fluctuations decreases as the prescribed length scale is reduced. Consequently, the respective energy spectra deviate from the target spectrum as the length scale is reduced. This aspect is more evident for the turbulence configurations T4-T7. Moreover, it is also observed that fluctuations are completely eliminated for the turbulence configuration T7, where the size of the finite elements cannot represent the corresponding length scale.
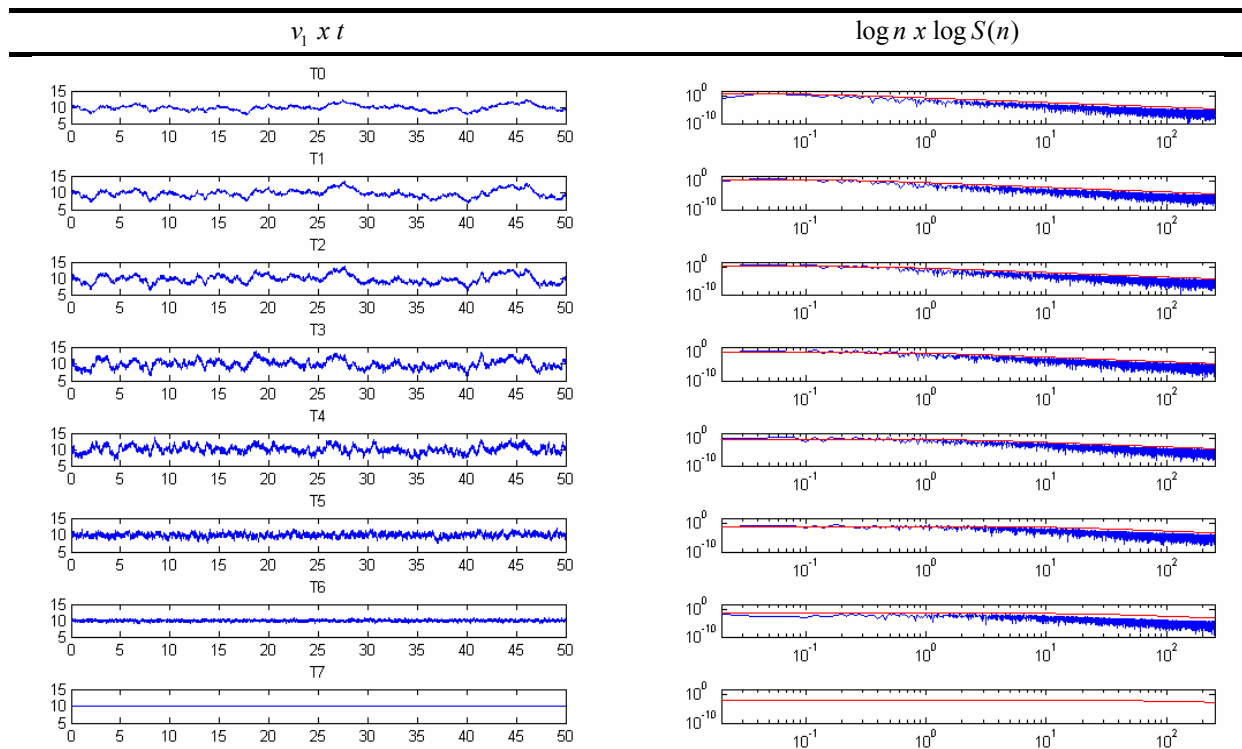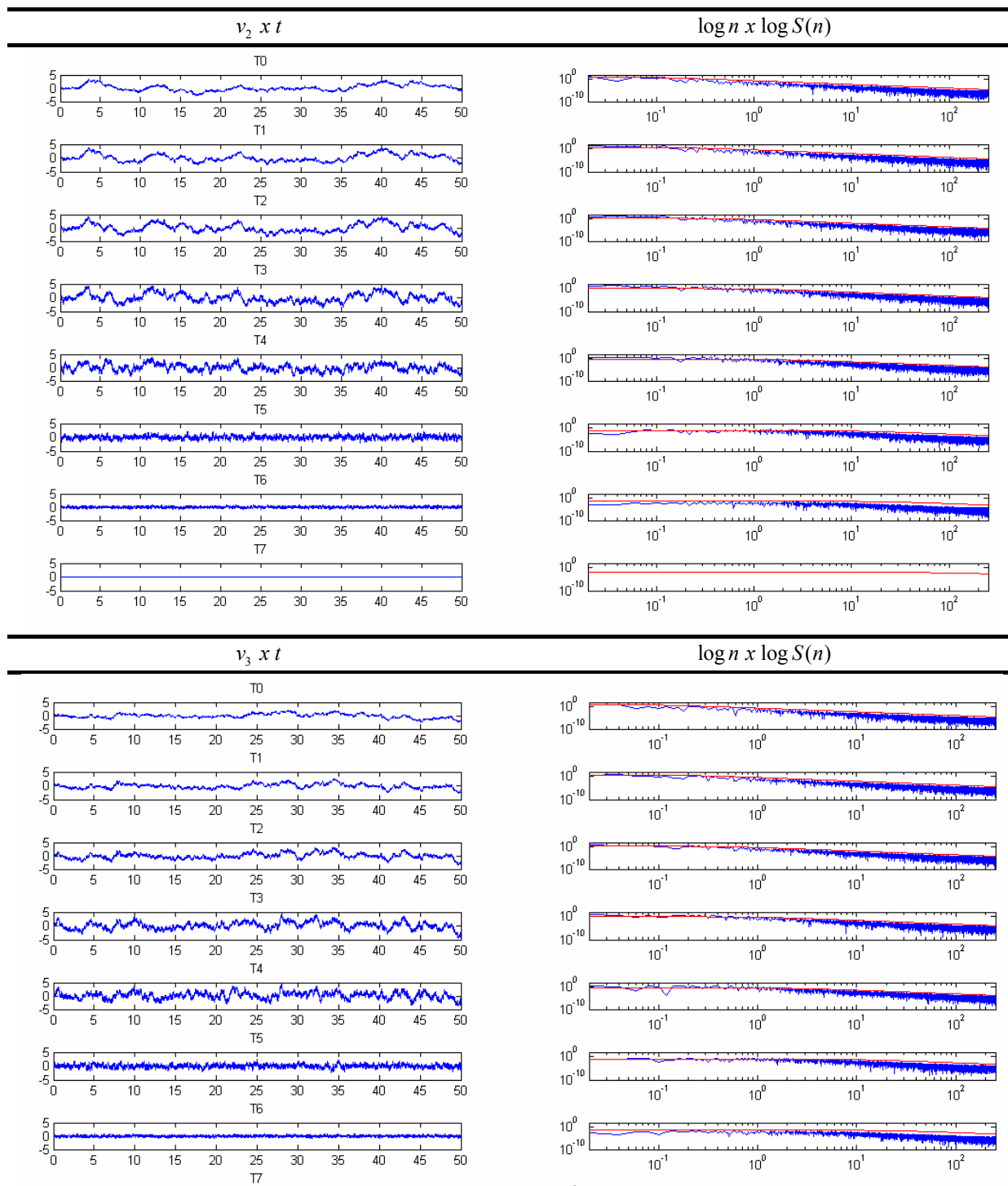
Figure 6. Time histories of the flow velocity components and the corresponding energy spectra obtained at the center point of the inflow plane ($x_1 = 0$ m; $x_2 = 5$ m; $x_3 = 5$ m).

Time histories of the flow velocity components and the corresponding energy spectra are now presented in Fig. 7 considering a measurement performed at the center point of the computational domain ($x_1 = 15$ m; $x_2 = 5$ m; $x_3 = 5$ m) referring to Mesh 1, where comparisons are performed taking into account the target spectrum described according to the von Karman model. The first 25 s of the velocity records were disregarded in the evaluation of the energy spectra to avoid the contribution of spurious oscillations observed in the

pressure field during the early stages of the numerical simulation. Results referring to the turbulence configuration T7 are not presented, whereas fluctuations are completely eliminated owing to the size of the finite elements. One can observe that the influence of numerical dissipation associated with grid refinement and the numerical model is now evidenced. The energy spectra obtained from the numerical predictions is significantly deviated from the target spectrum for the turbulence configurations T5 and T6. On the other hand, the low frequency range shows a good agreement with the von Karman model, mainly for turbulence configurations defined with larger length scales.
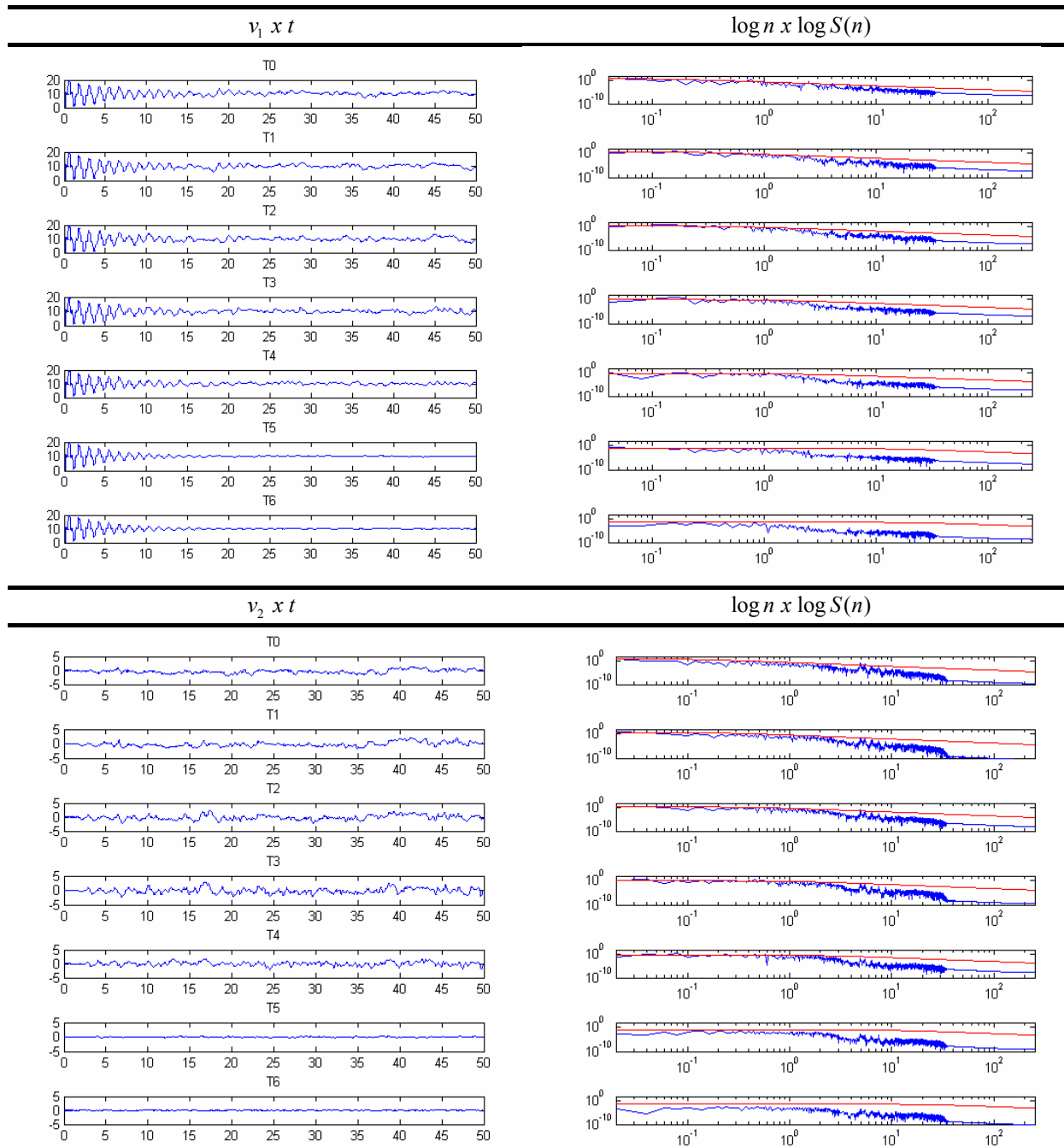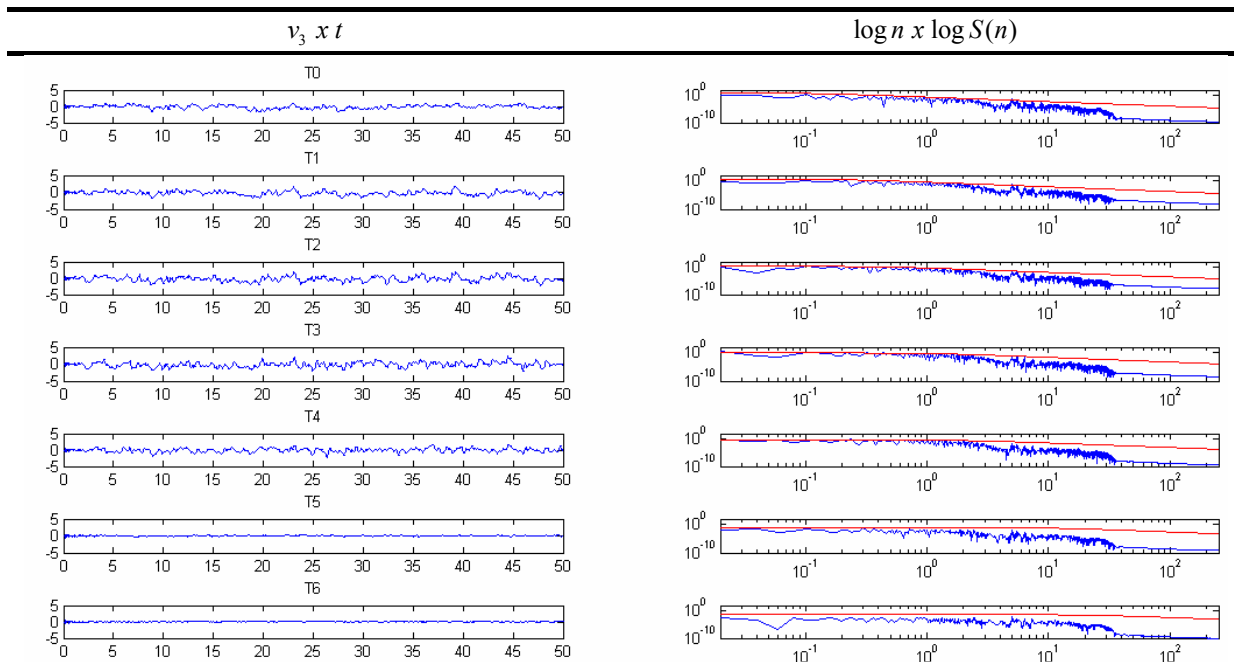
Figure 7. Time histories of the flow velocity components and the corresponding energy spectra obtained at the center point of the computational space (x_1 = 15 m; x_2 = 5 m; x_3 = 5 m).

Finally, time histories of the flow velocity components and the corresponding energy spectra are presented in Fig. 8 considering a measurement performed at the center point of the outflow plane (x_1 = 30 m; x_2 = 5 m; x_3 = 5 m). The finite element discretization refers to Mesh 1. Comparisons are carried out taking into account the target spectrum described according to the von Karman model. One can notice that the same aspects observed in the results referring to Fig. 6 are also valid for the predictions obtained here.
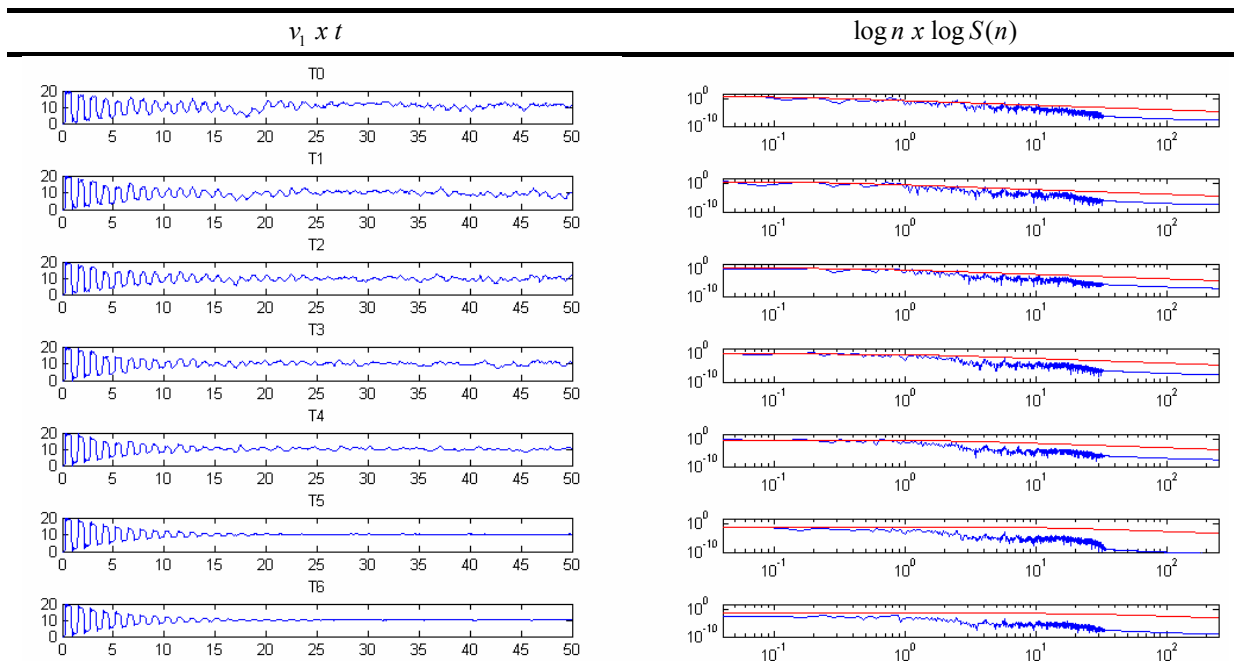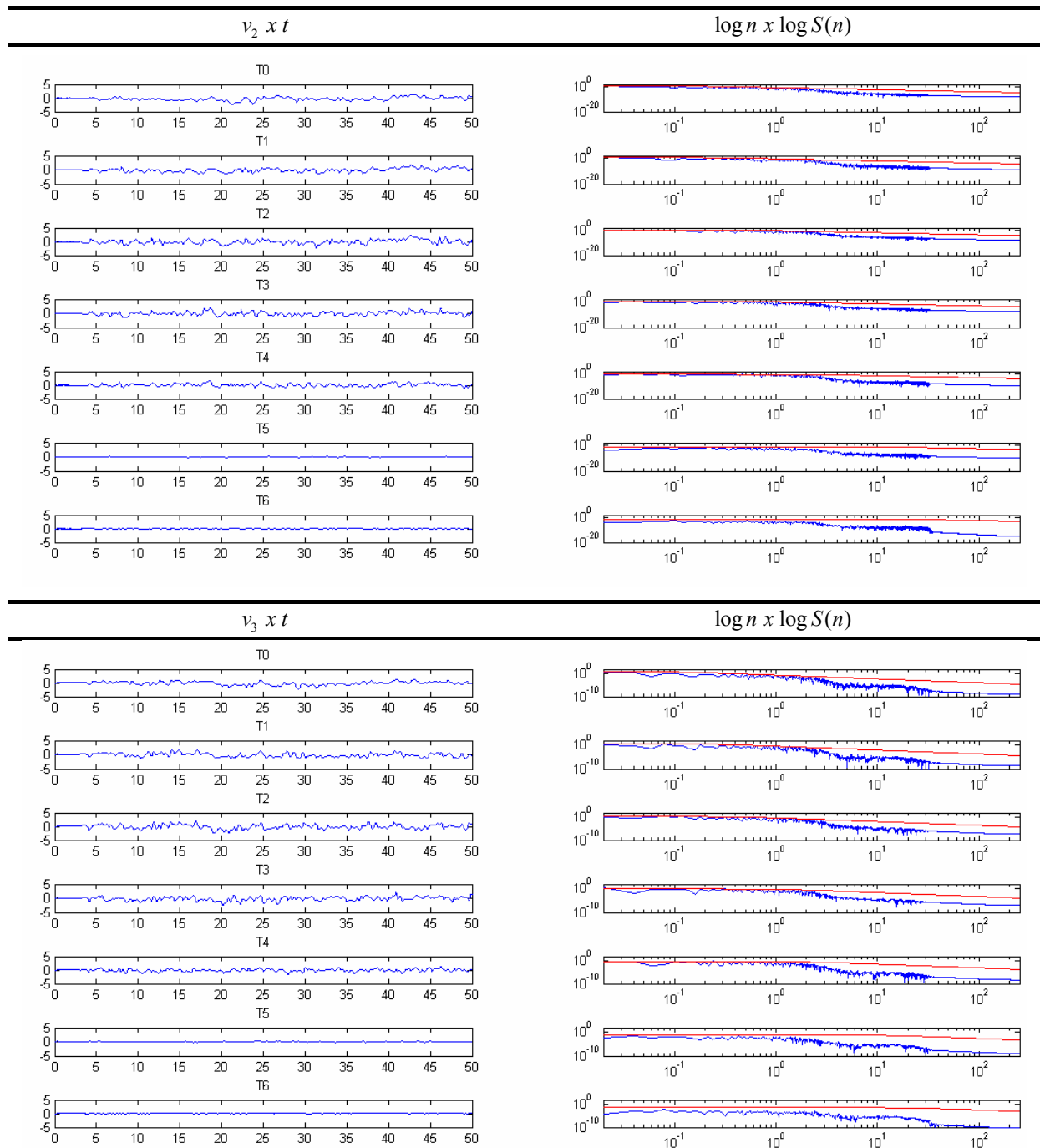
Figure 8. Time histories of the flow velocity components and the corresponding energy spectra obtained at the center point of the outflow plane ($x_1 = 30$ m; $x_2 = 5$ m; $x_3 = 5$ m).

The effects of the grid resolution over the turbulence generation can be evaluated with Fig. 9, where time histories of the flow velocity components and the respective energy spectra are compared with the target spectrum, which is represented according to the von Karman model. Only the turbulence configuration T1 was considered in this comparison. It is observed that the level of numerical dissipation is clearly smaller when Mesh 2 is utilized, which is evidenced considering that the corresponding energy spectra is less deviated from the target spectrum when compared with the energy spectrum obtained with Mesh 1. Some differences identified in the energy spectra referring to the velocity components may indicate the

influence of the symmetry boundary conditions adopted in the lateral and top walls and the constant pressure field imposed on the outflow plane of the computational domain. This aspect must be further investigated.

Velocity component x t	$\log n \ x \ \log S(n)$	$\log n \ x \ S(n)$	$\log \frac{n \cdot L_t}{\bar{U}} \ x \ \log \frac{n \cdot S(n)}{\sigma_u^2}$

$x_1 = 0 \ m$

$x_1 = 15 \ m$
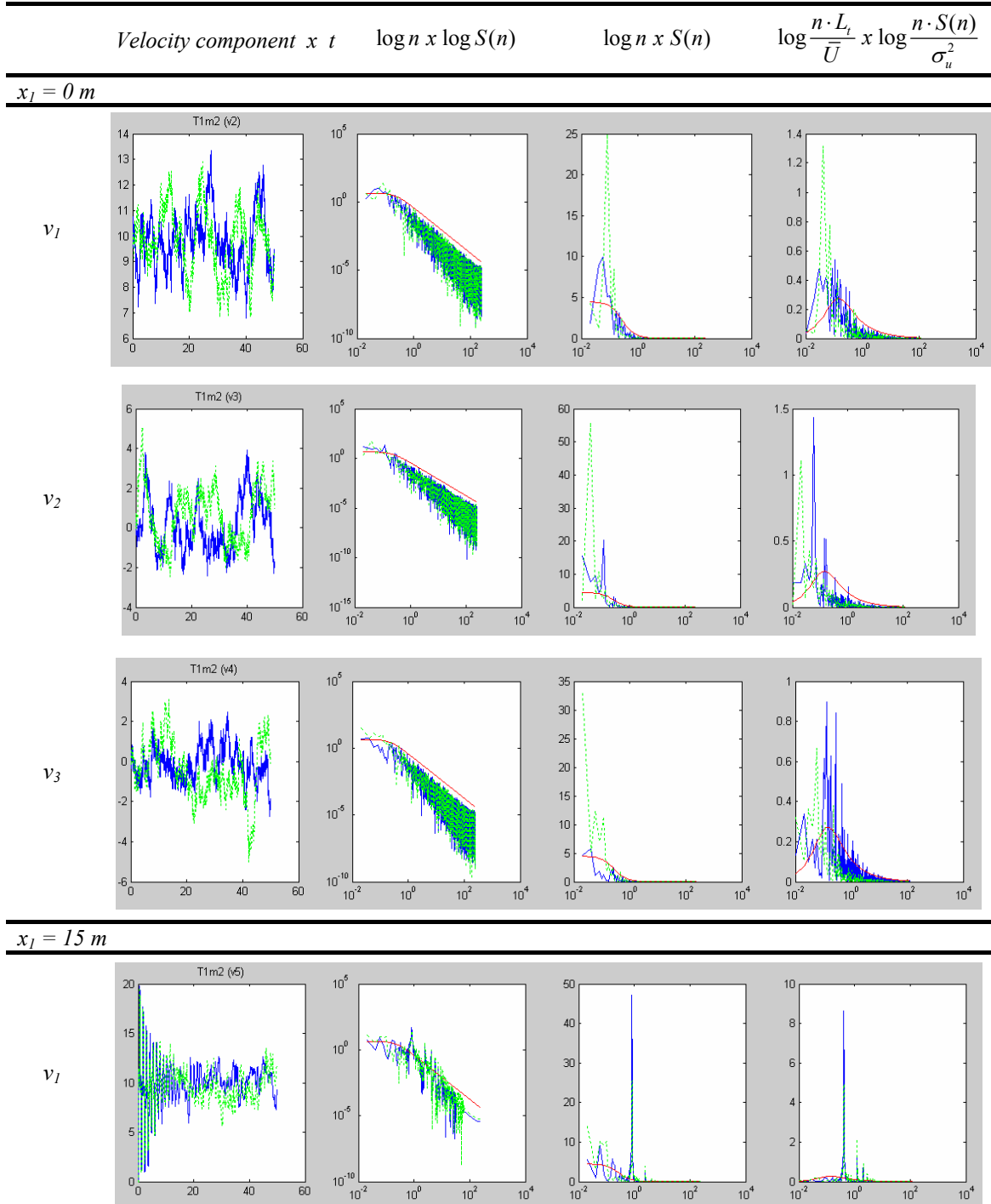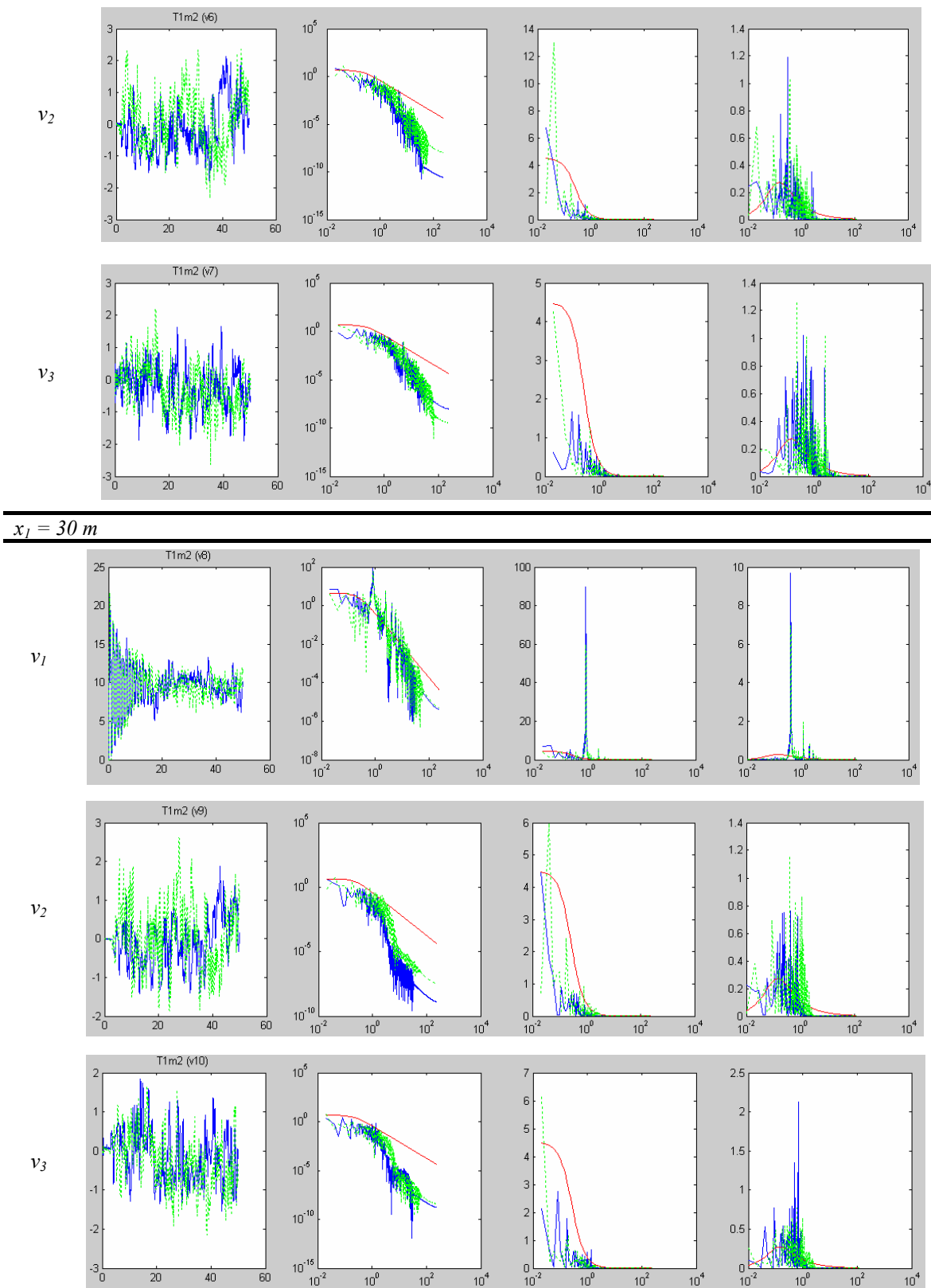
Figure 9. Effects of the grid resolution on the turbulence generation: results obtained with Mesh 1 (blue) and Mesh 2 (green).

A collection of turbulence statistical parameters referring to the numerical predictions obtained at the center point of the outflow plane ($x_1 = 30$ m; $x_2 = 5$ m; $x_3 = 5$ m) are reported in Table 3, where comparisons are performed with respect to the values specified initially ($V_1 = 10.0$ m/s and $Ix = Iy = Iz = 15\%$). In addition, profiles corresponding to the longitudinal component of the flow velocity vector are presented in Fig. 10, where three different positions along the longitudinal direction of the computational domain and the different turbulence configurations investigated here are considered. It is observed that the amplitude of variations around the time averaged values is reduced along the longitudinal direction of the computational domain, which indicates dissipation of the fluctuations produced on the inflow plane. Moreover, by analyzing Table 3 one can notice that RMS velocity components are better simulated if larger turbulence structures (length scale) are used. The large dissipation observed in the RMS velocity components v_2 and v_3 may be related to the symmetry boundary conditions adopted in the side and top walls of the computational domain.

Simulations	v_1		v_2		v_3	
	Mean	RMS	Mean	RMS	Mean	RMS
T0	11.02	1.21	-0.26	0.62	-0.09	0.62
T1	9.71	1.22	-0.08	0.63	-0.13	0.64
T2	9.70	1.06	-0.03	0.72	-0.10	0.77
T3	9.93	0.92	-0.04	0.61	-0.14	0.65
T4	10.05	0.69	0.07	0.50	-0.08	0.46
T5	10.13	0.15	0.00	0.09	0.04	0.09
T6	10.09	0.06	0.00	0.03	0.03	0.03

Table 3. Statistical results referring to turbulence fluctuations produced at the center point of the outflow plane ($x_1 = 30$ m; $x_2 = 5$ m; $x_3 = 5$ m).
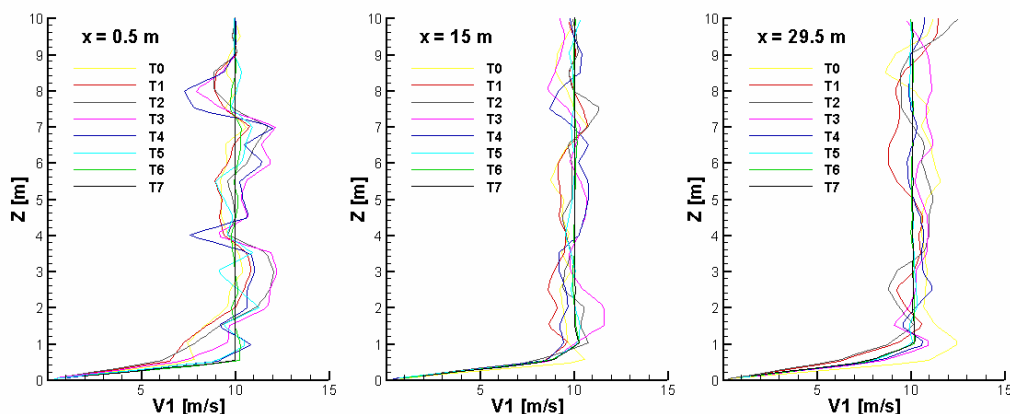
Figure 10. Profiles of the longitudinal component of the flow velocity vector along the longitudinal direction of the computational domain.

In order to illustrate the flow characteristic corresponding to the turbulent flow field developed with the turbulence generator model adopted in this work, instantaneous scalar fields of the velocity components v_1, v_2, v_3 and pressure p_s are presented in Fig. 11, which are associated with prediction obtained using the mesh configurations Mesh 1 and Mesh 2 and the turbulence configuration T1. Notice that the mesh configuration Mesh 2 can reproduce smaller turbulence structures, since the corresponding grid resolution is finer than that utilized by Mesh 1.

Mesh 1   Mesh 2

v_1

Mesh 1   Mesh 2

v_2

v_3

p_s
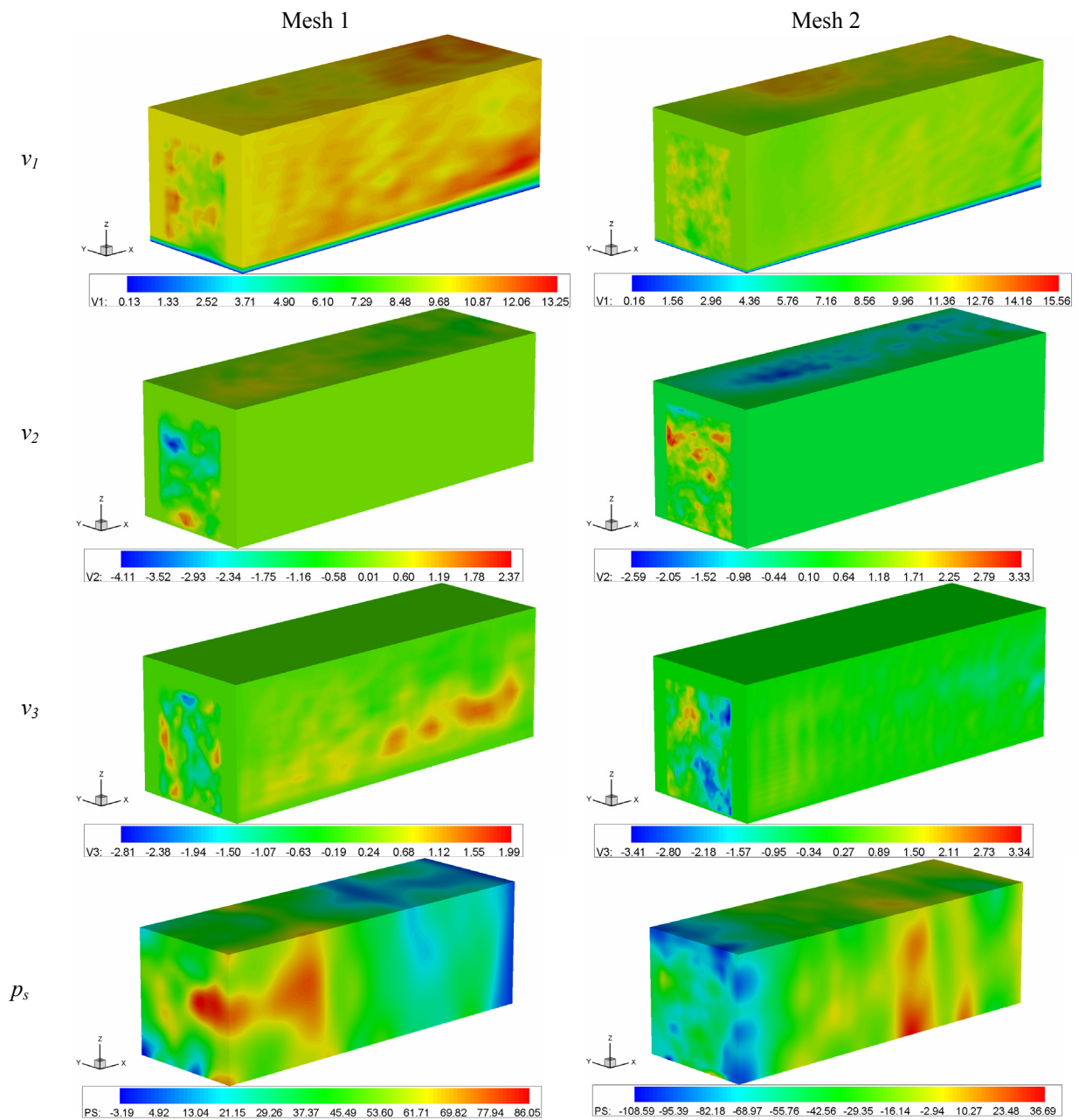
Figure 11. Instantaneous scalar fields of the velocity components v_1, v_2, v_3 and pressure p_s.

5.2 The Texas Tech University (TTU) building

The Texas Tech University (TTU) building model is analyzed here in order to validate the numerical scheme proposed in this work. This building model has been extensively investigated to validate wind tunnel experiments and CFD algorithms by using predictions obtained from full-scale measurements. The actual model presents the following geometric characteristics (see, for instance, Levitan et al., 1991; Levitan and Mehta, 1992): 9.1 m width (W), 13.7 m length (L), 4 m height (*H*) and a roof slope of 1.65°. In the present analysis, the direction of the wind flow is perpendicular to the lateral wall of the building, as illustrated in Fig. 12, where a detail of the finite element mesh employed near the model is also shown. Flow and geometric constants adopted in the numerical analysis are reported in Table 4, taking into account that the Reynolds number characterizing the flow is Re = 2.4×10^6.

Turbulence is simulated using LES with the Smagorinsky's sub-grid scale model, for which the dynamic coefficient is a fixed constant equal to $C_S = 0.12$.
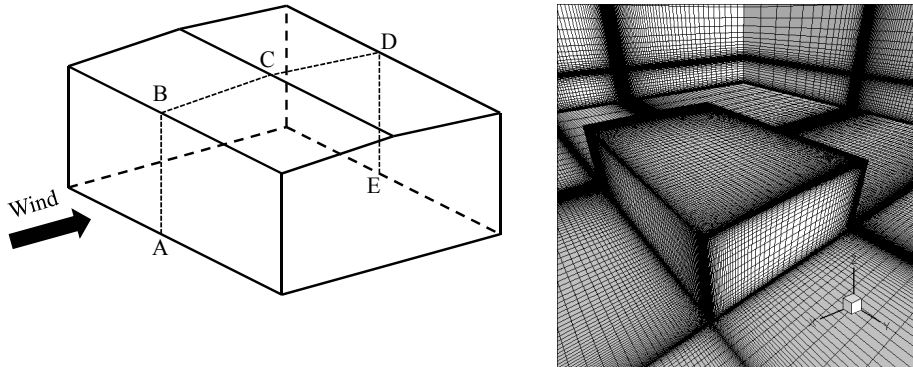
Figure 12: The TTU building model and the finite element mesh adopted in the present analysis.

Fluid specific mass (ρ)	1.0 kg/m^3
Kinematic viscosity (ν)	1.43×10^{-5} m^2/s
Sound speed (c)	53.75 m/s
Reference velocity – V_{ref} (z = 4m)	8.6 m/s
Characteristic dimension (W)	9.1 m
Time step (Δt)	2.5×10^{-4} s

Table 4. Flow and geometric constants utilized in the flow analysis over the TTU building model.

The computational grid utilized in the TTU building analysis was constructed considering 1502480 eight-node hexahedral elements. The smallest elements are located near the building model, presenting a characteristic dimension of 0.02 m. Symmetry boundary conditions are imposed on the side and top walls of the computational domain and no-slip condition is assumed on the ground and building surfaces. Constant pressure ($p = 0$) is prescribed on the outflow boundary and a mean velocity profile along the longitudinal direction is considered according to the following equation:

$$v_I = V_{ref}(z/H)^{0.18} \qquad (22)$$

where $V_{ref} = 8.6$m/s is the reference velocity at the height of the building (z = 4 m). By using the synthetic turbulence generator proposed in this work, turbulence fluctuations are generated since the beginning of the numerical simulation over a limited region of the inflow plane, which is defined considering the geometric parameters BDIST1 = 7 m and BDIST2 = 8 m (see Fig. 5 for geometric definitions on the region of inflow turbulence generation). A simplified approach is adopted here to define turbulence intensities along the Cartesian directions, where a uniform and isotropic distribution of 20% is considered. Three conditions are simulated: (a) no turbulence fluctuations; (b) turbulence fluctuations with length scale of $L_t = 2$ m; (c) turbulence fluctuations with length scale of $L_t = 4$ m.

The distribution of time averaged pressure coefficients over the building surface is shown in Fig. 13, where results obtained here are compared with results obtained from other authors. All predictions are referred to the intermediate plane of the building model (line A-B-C-D-E, see Fig. 12). One can observe that the inclusion of turbulence fluctuations in the incident flow modifies significantly the distribution of pressure over the building surface. A good

agreement is identified when both configurations for turbulence fluctuations are considered, although some significant differences can be found in the recirculation region above the roof surface, which indicate that the resolution of the finite element mesh must be improved in that region.
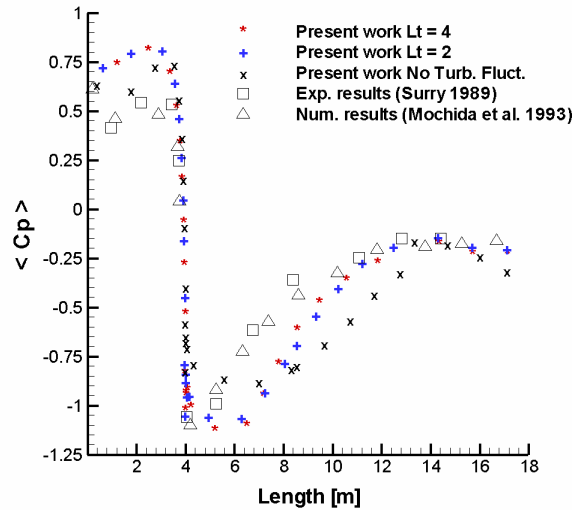
(A = 0; B = 4 m; C = 8,55 m; D = 13.1 m; E = 17.1 m)

Figure 13. Distribution of time averaged pressure coefficients over the building surface.

Some characteristics of the flow field can be observed from Fig. 14, where time average streamlines and pressure distribution over the intermediate plane of the computational domain (x_2 = 5 m) are presented for the different inflow turbulence configurations investigated here. The influence of the turbulence fluctuations on the flow reattachment above the building roof is clearly identified.
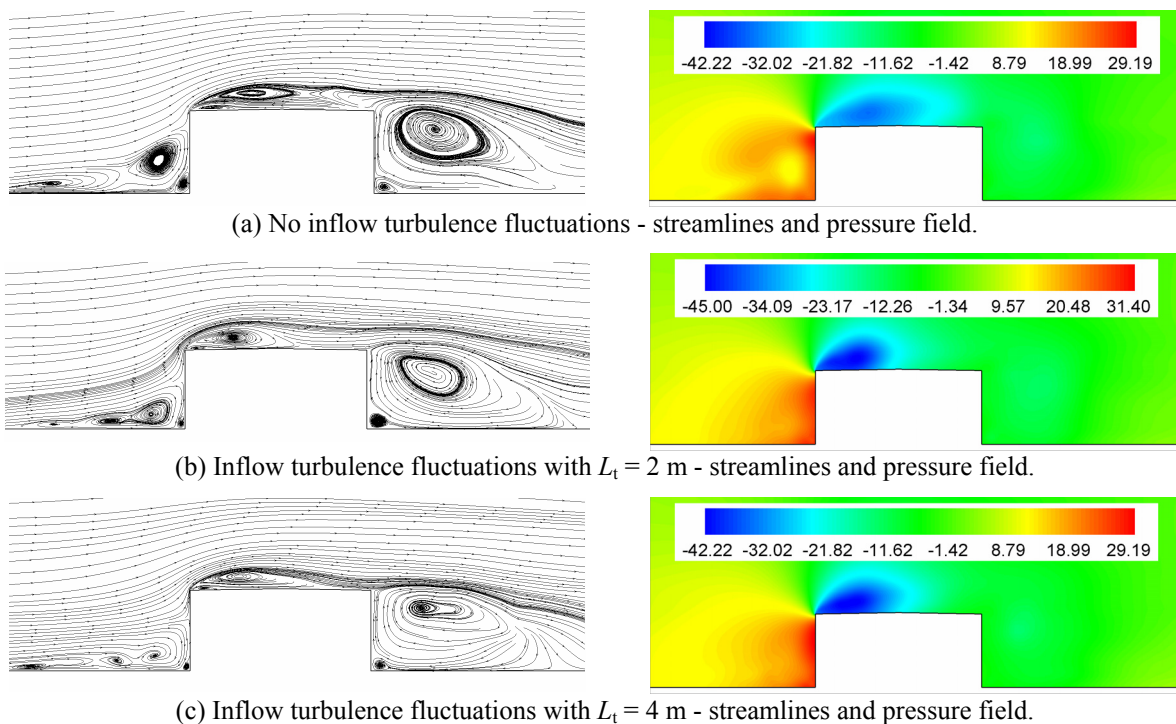
(a) No inflow turbulence fluctuations - streamlines and pressure field.

(b) Inflow turbulence fluctuations with L_t = 2 m - streamlines and pressure field.

(c) Inflow turbulence fluctuations with L_t = 4 m - streamlines and pressure field.

Figure 14. Time average streamlines and pressure fields obtained on the intermediate plane of the computational domain (x_2 = 26.85 m) for different inflow turbulence configurations.

Figure 15 shows instantaneous scalar fields (t = 30 s) corresponding to the flow velocity components v_1 and v_2, which were obtained considering the intermediate plane of the computational domain (x_2 = 26.85 m) and different inflow turbulence configurations. Results demonstrate that LES can produce turbulence fluctuations directly if an obstacle is positioned in the flow field (see Fig. 15a). On the other hand, when the algorithm for inflow turbulence generation is employed, turbulence fluctuations can be produced upstream the building position, which modify the flow configuration around the building (see Fig. 15a and 15b).

(a) No inflow turbulence fluctuations - v_1 and v_2.

(b) Inflow turbulence fluctuations with L_t = 2 m - v_1 and v_2.

(c) Inflow turbulence fluctuations with L_t = 4 m - v_1 and v_2.
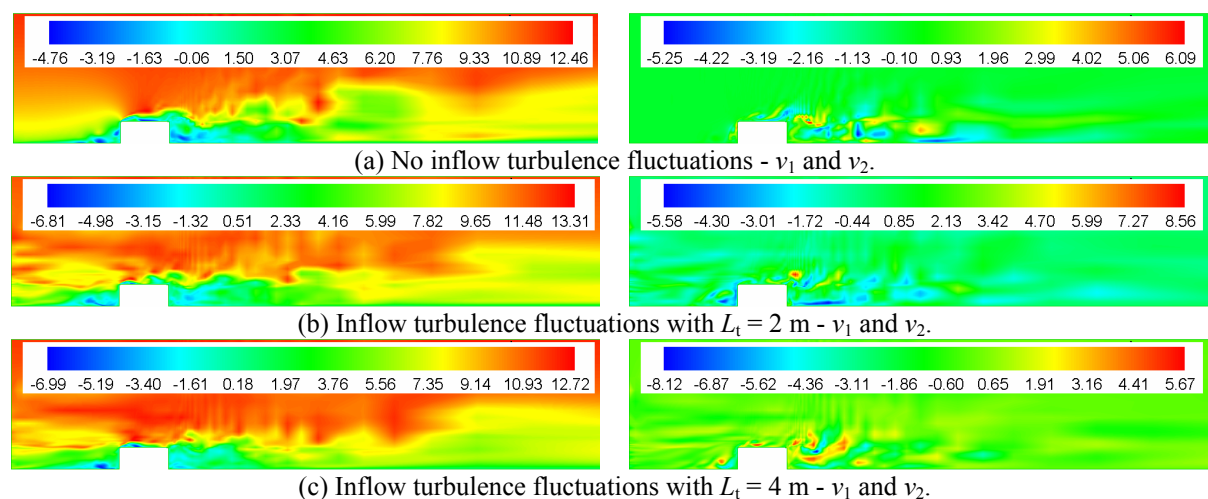
Figure 15. Instantaneous scalar fields of the velocity components v_1 and v_2 obtained on the intermediate plane of the computational domain (x_2 = 26.85 m) for different inflow turbulence configurations.

6   CONCLUSIONS

A numerical model based on Large Eddy Simulation (LES) and synthetic inflow turbulence was proposed in this work to investigate the influence of turbulence fluctuations over wind engineering flows. A finite element model was presented considering an eight-node hexahedral formulation for isothermal incompressible flows. The synthetic turbulence generator adopted in this work assumed homogeneous and isotropic turbulence as well as the divergence-free hypothesis. The numerical analyses carried out here demonstrate that the larger the turbulence structures (length scale), the lower the dissipation and the slower the decay of the turbulent energy. As smaller turbulence structures are generated, the inflow data becomes less and less correlated and the dissipation increases. One can conclude that the inflow structures to be generated must be properly discretized by the inlet mesh, even if their size is overestimated.

REFERENCES

Batten, P., Goldberg, U. and Chakravarthy, S. Interfacing statistical turbulence closures with large-eddy simulation. *AIAA Journal*, 42:485-492, 2004.

Billson, M., Eriksson, L.E. and Davidson, L. Modeling of synthetic anisotropic turbulence and its sound emission. In: *Proceedings of the 10th AIAA/CEAS Aeroacoustics Conference, AIAA 2004-2857*, Manchester, 2004.

Braun, A.L. Simulação Numérica na Engenharia do Vento incluindo Efeitos de Interação Fluido-Estrutura. DSc. Thesis, PPGEC/UFRGS, Porto Alegre, 2007.

Braun, A.L. and Awruch, A.M. Aerodynamic and aeroelastic analysis of bundled cables by numerical simulation. *Journal of Sound and Vibration*, 284:51-73, 2005.

Braun, A.L. and Awruch, A.M. Aerodynamic and aeroelastic analyses on the CAARC standard tall building model using numerical simulation. *Computers and Structures*, 87:564-581, 2009a.

Braun, A.L. and Awruch, A.M. A partitioned model for fluid-structure interaction problems using hexahedral finite elements with one-point quadrature. *International Journal for Numerical Methods in Engineering*, 79:505-549, 2009b.

Chorin, A.J. A numerical method for solving incompressible viscous flow problems. *Journal of Computational Physics*, 2:12-26, 1967.

Davenport, A.G. The spectrum of horizontal gushiness near the ground in high winds. *Journal of the Royal Meteorological Society*, 87:194-211, 1961.

Davidson, L. Using isotropic synthetic fluctuations as inlet boundary conditions for unsteady simulations. *Advances and Applications in Fluid Mechanics*, 1:1-35, 2007.

Germano, M., Piomelli, U., Moin, P. and Cabot, W.H. A dynamic subgrid-scale eddy viscosity model. *Physics of Fluids*, A3:1760-1765, 1991.

Hinze, J.O. *Turbulence*, 2nd Edition. McGraw-Hill: New York, 1975.

Hoshiya, M., 1972. Simulation of multi-correlated random processes and application to structural vibration problems. *Proceedings of JSCE*, 204:121-128.

Huang, S.H., Li, Q.S. and Wu, J.R. A general inflow turbulence generator for large eddy simulation. *Journal of Wind Engineering and Industrial Aerodynamics*, 98:600-617, 2010.

Jarrin, N., Benhamadouche, S., Laurence, D. and Prosser, R. A synthetic-eddy-method for generating inflow conditions for large-eddy simulations. *International Journal of Heat and Fluid Flow*, 27:585-593, 2006.

Kawahara, M. and Hirano, H. A finite element method for high Reynolds number viscous fluid flow using two step explicit scheme. *International Journal for Numerical Methods in Fluids*, 3:137-163, 1983.

Keating, A., Piomelli, U., Balaras, E. and Kaltenbach, H.J. A priori and a posteriori tests of inflow conditions for large-eddy simulation. *Physics of Fluids*, 16:4696-4712, 2004.

Klein, M.A., Sadkiki and Janicka, J. A digital filter based generation of inflow data for spatially developing direct numerical or large eddy simulations. *Journal of Computational Physics*, 186:652–665, 2003.

Kondo, K., Murakami, S. and Mochida, A. Generation of velocity fluctuations for inflow boundary condition of LES. *Journal of Wind Engineering and Industrial Aerodynamics*, 67&68:51–64, 1997.

Kraichnan, R. H. Diffusion by a random velocity field. *Physics of Fluids*, 13: 22-31, 1970.

Le, H. and Moin, P. *Direct numerical simulation of turbulent flow over a backward facing step*. Report nº TF-58, Stanford University, Dept. Mech. Eng., 1994.

Levitan, M.L., Mehta, K.C. Texas Tech field experiments for wind loads part 1: building and pressure measuring system. *Journal of Wind Engineering and Industrial Aerodynamics*, Amsterdam, 43:1615-1616, 1992.

Levitan, M.L., Mehta, K.C., Vann, W.P., Holmes, J.D. Field measurements of pressure on the Texas Tech Building. *Journal of Wind Engineering and Industrial Aerodynamics*, Amsterdam, 38:227-234, 1991.

Li, A., Ahmadi, G., Bayer, R. and Gaynes, M. Aerosol particle deposition in an obstructed turbulent duct flow. *Journal of Aerosol Science*, 25:91-112, 1994.

Lilly, D.K. A proposed modification of the Germano subgrid-scale closure method. *Physics of Fluids*, A4:633-635, 1992.

Liu, K.L. and Pletcher, R.H. Inflow conditions for the large eddy simulation of turbulent boundary layers: a dynamic recycling procedure. *Journal of Computational Physics*, 219:1-6, 2006.

Mochida, A., Murakami, S., Shoji, M. and Ishida, Y. Numerical simulation of the flowfield around Texas Tech Building by Large Eddy Simulation. *Journal of Wind Engineering and Industrial Aerodynamics*, 46&47:455-460, 1993.

Shinozuka, M. Simulation of multivariate and multi-dimensional random processes. *Journal of the Acoustical Society of America*, 49:357-367, 1971.

Shinozuka, M. and Jan, C.M. Digital simulation of random processes and its applications. *Journal of Sound and Vibration*, 25:111-128, 1972.

Simiu, E. and Scanlan, R.H. *Wind Effects on Structures*, 2nd Edition. John Wiley & Sons: New York, 1996.

Smagorinsky, J. General circulation experiments with the primitive equations, I, the basic experiment. *Monthly Weather Review*, 91:99-135, 1963.

Smirnov, R., Shi, S. and Celik, I. Random flow generation technique for large eddy simulations and particle-dynamics modeling. *Journal of Fluids Engineering*, 123:359-371, 2001.

Surry, D. Pressure measurements on the Texas Tech building (II), Wind tunnel measurements and comparisons with full scale. In: *Proceedings of 8th Colloquium on Industrial Aerodynamics*, Aachen, 1989.

Tamura, T. Towards practical use of LES in wind engineering. *Journal of Wind Engineering and Industrial Aerodynamics*, 96:1451-1471, 2008.

Tamura, T., Okuda, Y. and Okada, H. LES estimation of wind characteristics in the surface layer over various grounds-urban roughness effects and terrain effects. In: *Proceedings of the UJNR Panel on Wind and Seismic Effects (Task Committee D)*, Seattle, 2002.

White, F.M. *Viscous Fluid Flow*, 3rd Edition. McGraw-Hill: New York, 2005.

Zienckiewicz, O.C., Taylor, R.L. and Nithiarasu, P. *The Finite Element Method for Fluid Dynamics*, 6th Edition. Elsevier Butterworth-Heinemann: Oxford, 2005.